Kasetsart J. (Nat. Sci.) 38 : 157 - 178 (2004)

Properties Enhancement of Short-Glass-Fiber Reinforced Thermoplastics by Sandwich Injection Molding Technique

Somjate Patcharaphun[1] and Günter Mennig[2]

ABSTRACT

This article demonstrates the possibility of using sandwich injection molding in order to improve the mechanical properties of short-glass-fiber-reinforced thermoplastic by investigating the effect of fiber orientation, compared with conventional injection molding. The effects of short-glass-fiber content within skin and core materials, in the present case PP, varying from 0 to 40 wt % were studied. The results showed an increase in the maximum tensile stress and impact strength as the concentration of the short-glass-fiber was increased. The mechanical properties of sandwich moldings were observed to be slightly higher than conventional injection moldings, which is attributed to the higher fiber orientation and lesser voids within the core layer. The effect of different processing types on the phase distribution of short-glass-fibers showed no significant phase separation effects between sandwich and conventional injection molding processes, except when using of sandwich injection process with different materials. The results obtained by analyzing the fiber attrition inside the skin and core regions in the longitude direction of tensile specimens showed that the degree of fiber degradation inside the skin layers were higher than the core layers and there are only minor differences in fiber length inside skin regions observed between sandwich and conventional injection molding processes, whilst this effect being more pronounced in the core regions and for the higher fiber volume fraction. The theoretically calculated values of the ultimate tensile stress (UTS) were found to be considerably higher than the experimental values. However, a more realistic estimation of UTS can be achieved by using measured values for fiber length within skin and core layers.

Key words: sandwich injection molding, fiber orientation, fiber length distribution, short-glass-fiber, mechanical properties

INTRODUCTION

At present, the use of composite materials in industry is well accepted and increasing every years. Both thermoset and thermoplastic polymers are used in combination with glass fibers (chopped strand, continuous, etc.). The main advantage of composites over steel is higher strength to weight ratio and remarkably enhanced physical properties when compared with pure polymer products. The other benefits are ease of processing, design freedom, high impact and corrosion resistance.

Recently, thermoplastic composites play an important role because of their greater ductility and processing speed, as compared to thermosets. They are frequently used as matrices of short-

1 Department of Material Engineering, Faculty of Engineering, Kasetsart University, Bangkok 10900, Thailand.
2 Institut für Allgemeinen Maschinenbau und Kunststofftechnik, Techniche Universität Chemnitz, Chemnitz 09107, Germany.

fiber-reinforced thermoplastics (SFRT). Although SFRT do not achieve the characteristic mechanical values which can be obtained by long-fiber reinforcement (Thomson, 2002; Regan *et al*., 1995.) but they can still be processed in convenient way and their excellent price/property ratio, e.g. by using the injection molding of these composites for the high volume production purposes, complex shapes, and lower manufacturing costs. Furthermore, their intrinsic recyclability is rapidly being recognized as a strong driving force for their further application (Clegg, 1994). However, the properties of short-fiber-reinforced thermoplastics are posing a problem of fiber orientation depending on processing conditions such as velocity, pressure, temperature, and by mold design such as gating, inserts and section thickness (Akay and Barkley, 1985; Gupta dnd Wang, 1993.) as schematically demonstrated in Figure 1. Therefore, these materials cannot be assumed to possess isotropic mechanical properties. The different fiber orientation between skin and core layer affects the mechanical and thermal properties of the molding and can also lead to distortion due to differential shrinkage between sections with different fiber orientations (Bailey, 1994).

The two-component injection molding process (sandwich molding process) is shown in Figure 2, consists of two injection units and the different polymer melts are injected sequentially into a cold mold. The first polymer entering into the mold to be the skin material of the final part, and the core material is embedded within the solidified layers. The advantage of this process over single-component injection molding process are recycled polymer that can be used as core material within skin materials and cellular polymer can be used as core material to reduce part weight and part residual stress. A number of papers (Chen *et al*. 1994; Schlatter *et al*., 1999) have been published concerning the polymer melt flow and weldline strength of injection molding carried out using co-injection molding technique whilst little attention has been given to the effect of molding parameters on mechanical properties of co-injection molding. Seldezn (Seldezn, 2000) studied the effect of molding conditions on material distribution and mechanical properties of a sandwich molded plate in co-injection molding using a polyamide 6 (PA6) as skin and a 20% glass-fiber-reinforced polybutyleneterephtalate (PBTP) as core. The results suggested that three parameters: injection velocity, core temperature, and core content were the most significant affecting skin / core distribution. A high core temperature was the most significant variable promoting a constant core thickness, while core content was the most significant factor influencing a

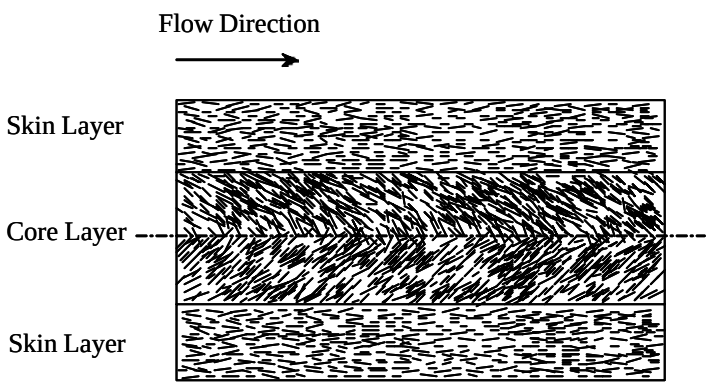

Figure 1 Schematic diagram of an injection molding indicating the fiber orientation in the skin and core layers.

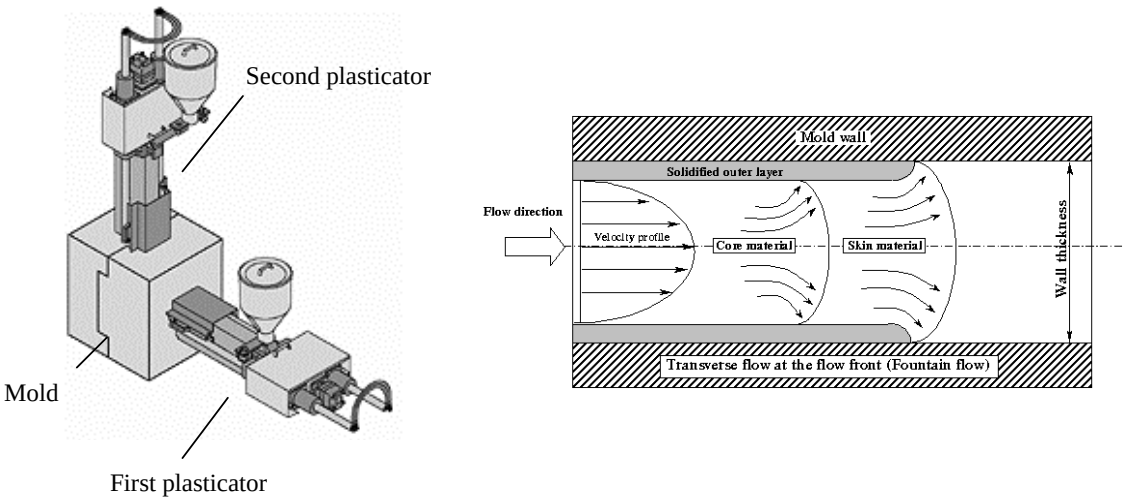

Figure 2 (a) Schematic principle of sandwich injection molding process and (b) Polymer melt flow profile in sandwich molding.

breakthrough of the core. Impact and flexural properties show a high correlation with the skin / core distribution in the thickness direction. An increased core thickness increases flexural modulus and strength but trend to decreasing in impact strength due to the brittle core and propagates through the ductile skins. The SCORIM^{TM} method, which has been developed by Allan and Bevis (Allan and Bevis, 1994) can control the fiber orientation of injection molded parts using a two live–feed device which is located between the plastification unit and the mould cavity. The experimental results of which were also compared with those of parts made by conventional molding. Their finding shows that shear controlled orientation technology (Scortec) can enhance fiber alignment and tensile modulus when measured parallel to the process.

Since the fiber orientation distribution is critical to the mechanical performance in discontinuous fiber composites. Therefore, the objective of this work, the sandwich injection molding technique is used in order to enhance the mechanical properties of short-glass-fiber-reinforced thermoplastics. The effects of fiber concentration (ranging from 0 to 40 wt %), fiber orientation, phase separation, and fiber length distribution within skin and core layer on tensile and impact strength were our primary focus. The experimental results of which are then compared with those obtained from conventional injection molding machine and theoretical calculation of ultimate tensile strength (UTS) based on a rule of mixture for short fiber composite.

MATERIAL AND METHOD

Materials used in this study were unfilled polypropylene (PP-H 1100 L), supplied in granular form by TARGOR and polypropylene filled with 20 and 40 wt % short-glass-fiber (PP32G10-0 and PP34G10-9) marketed by BUNA. The test specimens were molded on an ARBURG ALLROUNDER two-component injection molding machine (Model: 320S 500-350). It can be employed both for conventional injection molding and sandwich molding. The core materials were colored prior to injection molding, to facilitate

identification of the interface between the two materials. Levels for injection speed and skin/core volume ratio were chosen by trial and error such as: the injection speed of first plasticator (skin material) should be high in order to achieve a good surface finish and to prevent premature solidification of the melt (Zoltex, 2000) whereas, lower injection speed of second plasticator (core material) was used to assess the uniform core extension along the flow direction without the breakthrough of the core material at the far end of the bar (Schlatter *et al*., 1999; Seldezn, 2000). Several settings were tried and those leading to an overall satisfying quality with regard to visual properties were finally chosen, as shown in Figure 3. All the specimens were molded only after the machine had attained steady state with respect to the preset melt and mold temperatures. The mold temperature was 55°C and the five heating zones (from nozzle to feed zone) were set to 250°C, 240° C, 230°C, 220°C, and 210°C, respectively. The processing parameters were summarized in Table 1 and the experimental outlines for investigating of single and sandwich molding specimens, containing different short-glass-fiber contents between skin and core materials, are given in Table 2.

The molded tensile specimens were tested on Zwick 1464 mechanical tester at a crosshead speed of 5 mm/min for a sample gage length of 50 mm, according to the recommendation of DIN EN ISO 527-1/1A/5. For each molding condition, five dumbbell-shaped specimens were tested and the average values of the maximum tensile stress were used for analysis.

Charpy impact tests were conducted on a CEAST impact tester model 6545 using the specimens with a V-notch. The tests were carried out with impact energy of 1 Joule and a sample span length of 80 mm, referring to the standard of DIN EN ISO 179/1 e A. The average values of notched impact strength (kJ/m^2) were obtained again from group of five specimens.

The fiber orientation distribution and area

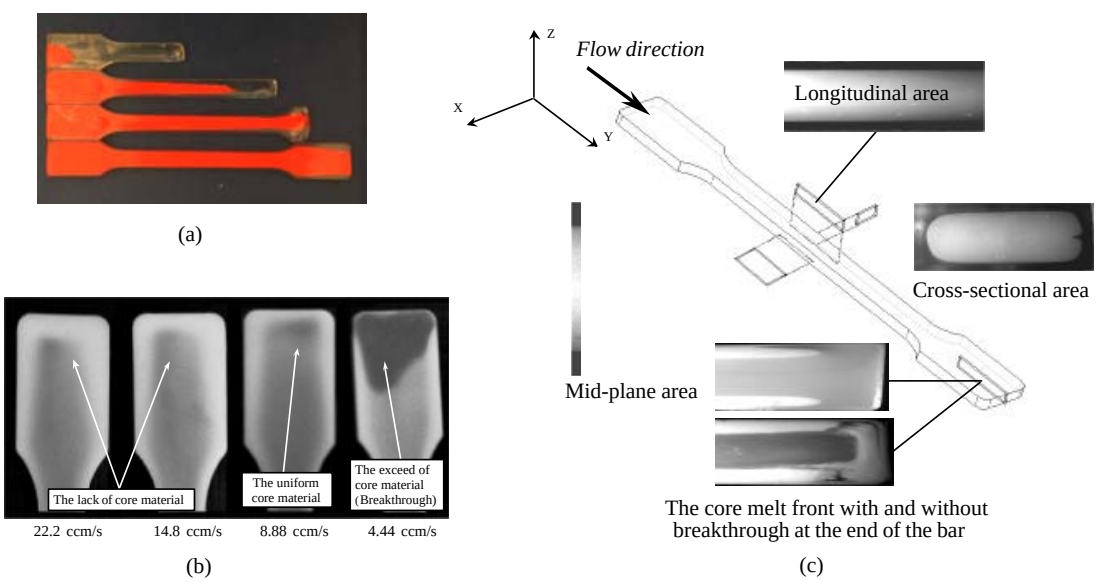

Figure 3 (a) Isochrones in sandwich injection molded short shots at different times, (b) Flow patterns in the region of the far end of the tensile bar at different injection flow rates of core material, and (c) Location of cross-sectional and longitudinal areas for this investigation.

fraction between skin and core layers were assessed by OLYMPUS model PMG3 optical microscopy and computer aided image analysis (a4i Analysis version 5.1 and Image-Pro Plus). The specimens for the observation of fiber orientation were obtained from tensile test piece by cutting at the center of the specimen, as illustrated in Figure 2 (c), and mounting the section of parts on a stage, which were then polished by a metallurgical polishing technique. The average fiber orientation factor, f_p in the skin and core regions (f_{ps} and f_{pc}, respectively) were calculated using equations 1a and 1b (Karger - Koscis, 1989).

$$f_p = 2\langle \cos^2 \varphi \rangle - 1 \quad (1a)$$

$$\left\langle \cos^2 \varphi \right\rangle = \frac{\sum_i N(\varphi_i) \cos^2\left(\varphi_i^2\right)}{\sum_i N(\varphi_i)} \quad (1b)$$

where φ_i is the angle between the individual fibers and local flow direction, and $N(\varphi_i)$ is the number of fibers with a certain angle φ_i to the local flow direction. This orientation function takes values between –1 when all the fibers are

Table 1 Processing conditions.

Conditions	Single molding	Sandwich molding	
		1st-plasticator	2nd-plasticator
Injection pressure (bar)	1000	1000	1000
Holding pressure (bar)	800	-	800
Holding time (sec)	10.8	-	10.8
Back pressure (bar)	60	60	60
Cooling time (sec)	36	-	36
Injection flow time (sec)	0.80	0.80	3.0
Screw speed (m/min)	12	12	12
Injection volume (ccm), (%)	37 (100%)	14.8 (40%)	22.2 (60%)

Table 2 Experimental outlines in this study.

No.	Single molding		Sample code
1	PP		PP
2	PP+SGF 20 wt%		SFRPP20
3	PP+SGF 40 wt%		SFRPP40
	Sandwich molding		Sample code
	Skin material	Core material	(Skin/Core)
4	PP+SGF 20 wt%	PP	SFRPP20/PP
5	PP	PP+SGF 20 wt%	PP/SFRPP20
6	PP+SGF 20 wt%	PP+SGF 20 wt%	SFRPP20/SFRPP20
7	PP+SGF 40 wt%	PP	SFRPP40/PP
8	PP	PP+SGF 40 wt%	PP/SFRPP40
9	PP+SGF 40 wt%	PP+SGF 20 wt%	SFRPP40/SFRPP20
10	PP+SGF 40 wt%	PP+SGF 40 wt%	SFRPP40/SFRPP40

perpendicular to the flow and 1 when all the fibers are parallel to the flow. In the case of random orientation, the value is 0.

For the investigation of fiber length within skin and core layer, the tensile specimen were cut into seven pieces, as indicated in Figure 4 and the separation of skin and core materials were utilized by microtome technique. Short-glass-fibers were then isolated from the composite materials by pyrolysis at the temperature of 650°C in a muffle furnace for about 1 hour. Ash of fibrous material was left and some fibers were extracted from the sample ash and dispersed on a rectangular glass plate. The plate was placed on the observation stage of a microscope. Magnified fiber images were transmitted to a suitable magnification (×50), and fiber images were then semi-automatically digitized by Image-Pro Plus software with a PC. The fiber length distributions (FLD) were determined by number-average fiber lengths which calculated from a minimum of 500 length measurements on fibers recovered from incineration of subdivision parts and individual layers. The percentage of the differences between a number-average fiber length of pellets and the overall glass fiber length inside the molded part ($\%\Delta l$) was used to describe the results, which can be considered using the following equation:

$$\%\Delta l = \left[\frac{l_j - l_G}{l_G}\right] \times 100 \qquad (2)$$

with l_G being the number-average fiber length inside the granule and l_j is the local fiber length inside the individual layers (skin and core layers) of sectioned parts

The phase separation analysis of sandwich and single molding processes were determined using a burning-off method according to DIN EN 60. The same subdivision as shown in Figure 4 was selected. The statistical calculation and the experimental procedure were employed in accordance with the work carried out by Hegler et al. [24]. The percentage of the differences between the local filler concentration of sectioned part and the overall glass content inside the molded part ($\%\Delta M_j$) was used to illustrate the results, which can be determined using the following equation:

$$\%\Delta M_j = \left[\frac{M_j - M_{tot}}{M_{tot}}\right] \times 100 \qquad (3)$$

where M_j is the local filler content and M_{tot} is the average total mass of specimen, which is calculated by Equation 2.

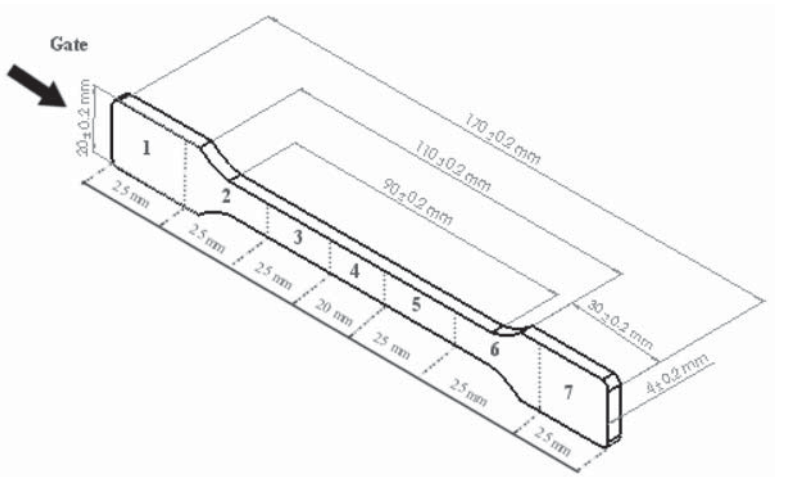

Figure 4 Subdivision of dumbbell specimen for fiber length measurement and phase distribution analysis.

$$M_{tot} = \frac{1}{n}\sum_{i}^{n}\left[\frac{\sum_{j} m_G}{\sum_{j} m_P}\right], \; j = 1,\ldots\ldots,7 \quad (4)$$

where m_P is the weight of specimen prior to burning off, m_G is the weight of the remaining glass, and is the number of samples ($n \geq 5$).

RESULTS AND DISCUSSION

Fiber Orientation Distribution

Single molding and a simple type of mold cavity were considered to study fiber orientation distribution. The skin and the core were easily observed in longitudinal direction to the flow in the skin and a perpendicular orientation to the skin in the core. This has been observed also in other studies (Gogos *et al*., 1986; Akay and Barkley, 1991; Gupta and Wang, 1993; Allan and Bevis, 1994). In the skin region, the fiber orientation is predominately along the flow direction due to the elongational forces developed during fountain flow at the front and the shear flow after the front has passed (Gogos *et al*., 1986; Tadmor, 1974). In contrast, the core region consists of random-in-plane fiber alignment caused by differential solidification, shearing, and melt-flow patterns (Bailey, 1994), as illustrated in Figures 5 and 6. Micrographs clearly revealed that the fibers orient along the parabolic profile in a plane parallel to the z-y plane in agreement with a fountain flow behavior and the voids which are mostly localized within the core layer where fiber orientation changes rapidly due to divergent flow (Akay and Barkley, 1991; Meddad and Fiba, 1995). It was also seen that the value of average fiber orientation factor within the core layer (f_{pc}) of SFRPP20 was higher than that of SFRPP40 (Table 3). In addition, the results obtained from Image-Pro Plus Analysis software also indicated that the area fraction between core layer and cross-sectional area of SFRPP20 being about 8%, whereas SFRPP40 representing about 17%. The results are in good agreement with the work carried out by Karger-Kocsis and Friedrich, (1987, 1988) in such a way that an increase in core layer structure of injection molded short-fiber-reinforced thermoplastics appears to be more pronounced as the glass fiber content increases.

Figure 7 and 8 show the fiber orientation inside the skin and core layers of sandwich molded

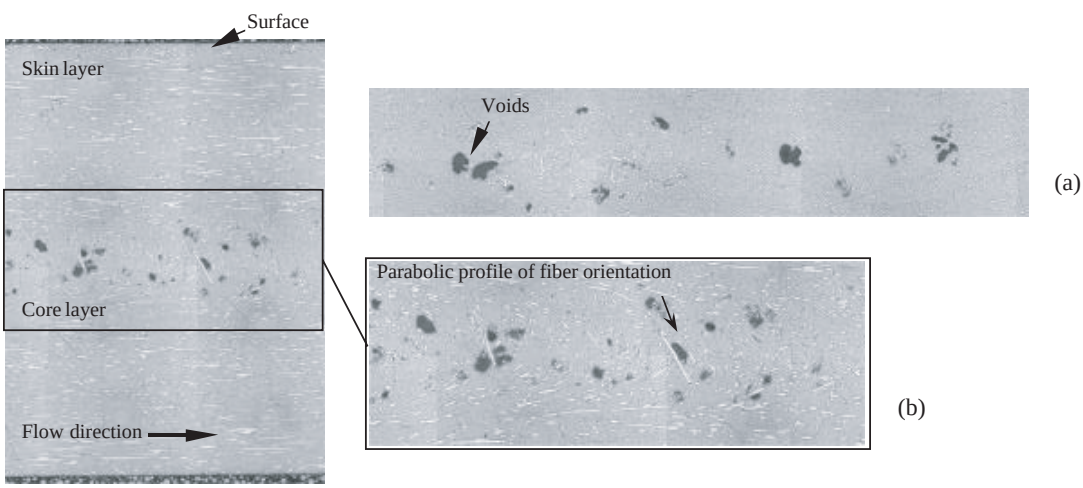

Figure 5 Optical micrographs in the z-y plane of SFRPP20: (a) Cross-sectional and (b) Longitudinal area in the center of the specimen.

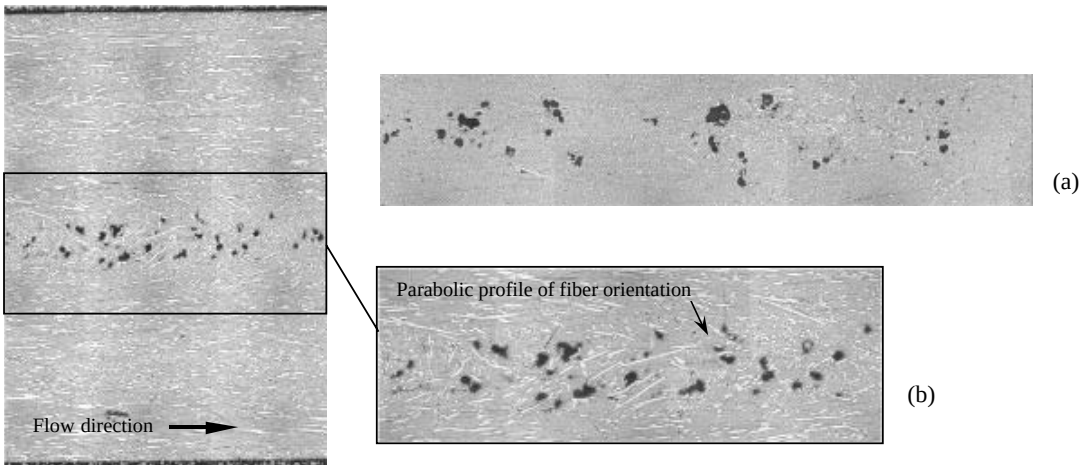

Figure 6 Optical micrographs in the z-y plane of SFRPP40: (a) Cross-sectional and (b) Longitudinal area in the center of the specimen.

Table 3 Average fiber orientation factor, , in the skin and core regions of short-glass-fiber-reinforced PP.

Specimens	Fiber orientation factor	
	f_{ps}	f_{pc}
SFRPP20	0.94	0.65
SFRPP40	0.98	0.57
SFRPP20/SFRPP20	0.98	0.96
SFRPP40/SFRPP40	0.99	0.95
SFRPP20/PP	0.99	_
SFRPP40/PP	0.97	_
PP/SFRPP20	_	0.87
PP/SFRPP40	_	0.83
SFRPP40/SFRPP20	0.98	0.92

specimens containing different glass-fiber contents. For the SFRPP20/SFRPP20 and SFRPP40/SFRPP40, the absolute values of f_{pc} along the flow direction within core layer were higher than those obtained from conventional injection molding, as expected. In terms of the area fraction between core layer and cross-sectional area, the results also indicated that the area fraction of SFRPP20 and SFRPP40 were reduced to 4%. The explanation for these would result from two sources: First, it was due to the skin material of sandwich molding which was first cool and solidified as it comes into contact with the cold mold wall, while the core material still exists at the center of the flow channel. Therefore, the solid skin material might act as the second mold wall inside the mold cavity resulting in the width of the flow channel becoming narrower. This behavior was supported by previous work

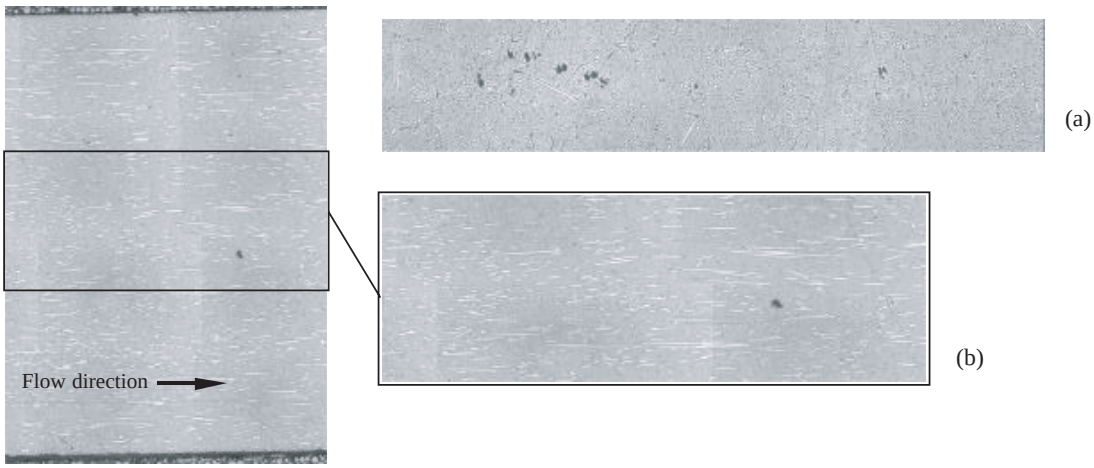

Figure 7 Optical micrographs in the z-y plane of SFRPP20/SFRPP20: (a) Cross-sectional and (b) Longitudinal area in the center of the specimen.

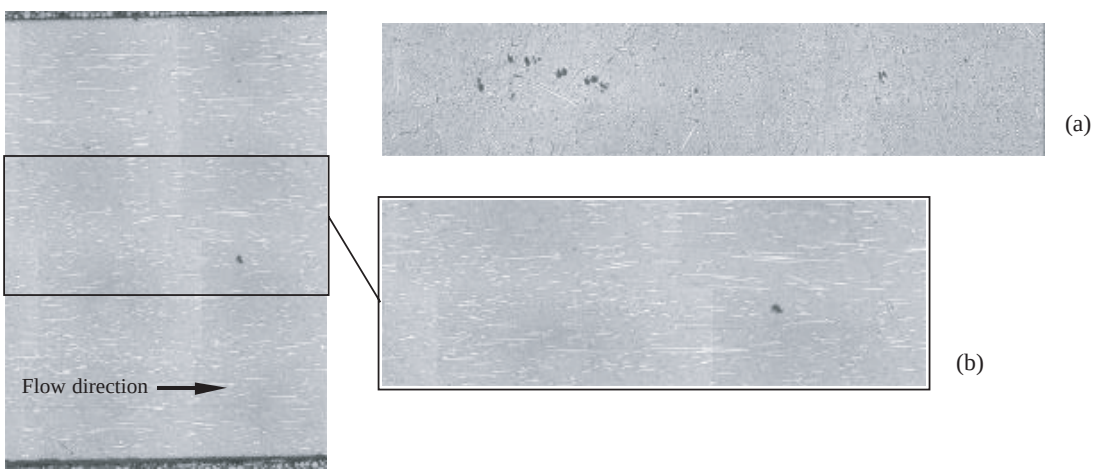

Figure 8 Optical micrographs in the z-y plane of SFRPP40/SFRPP40: (a) Cross-sectional and (b) Longitudinal area in the center of the specimen.

carried out by Akay and Barkley (1991) and Pechulis and Vautour (1997), dealing with the core thickness and the presence of voids which increased with increasing the thickness of molding which significantly divergent flow occurring in the mold cavity. Second, the slower the injection speed of the second material, the higher the thickness of solid layer formed during the filling stage, which restricts the cross-sectional area available for the flowing melt. This leads to a higher velocity gradient that tends to increase the orientation at the adjacent melt layer. Theses observations are also in accordance with those of Gupta and Wang (1993) as well as Gerard *et al*. (1998) in that the increasing the thickness of cold boundary layer, fibers at the mid-plane become more flow-aligned and the thickness of the core region decreases.

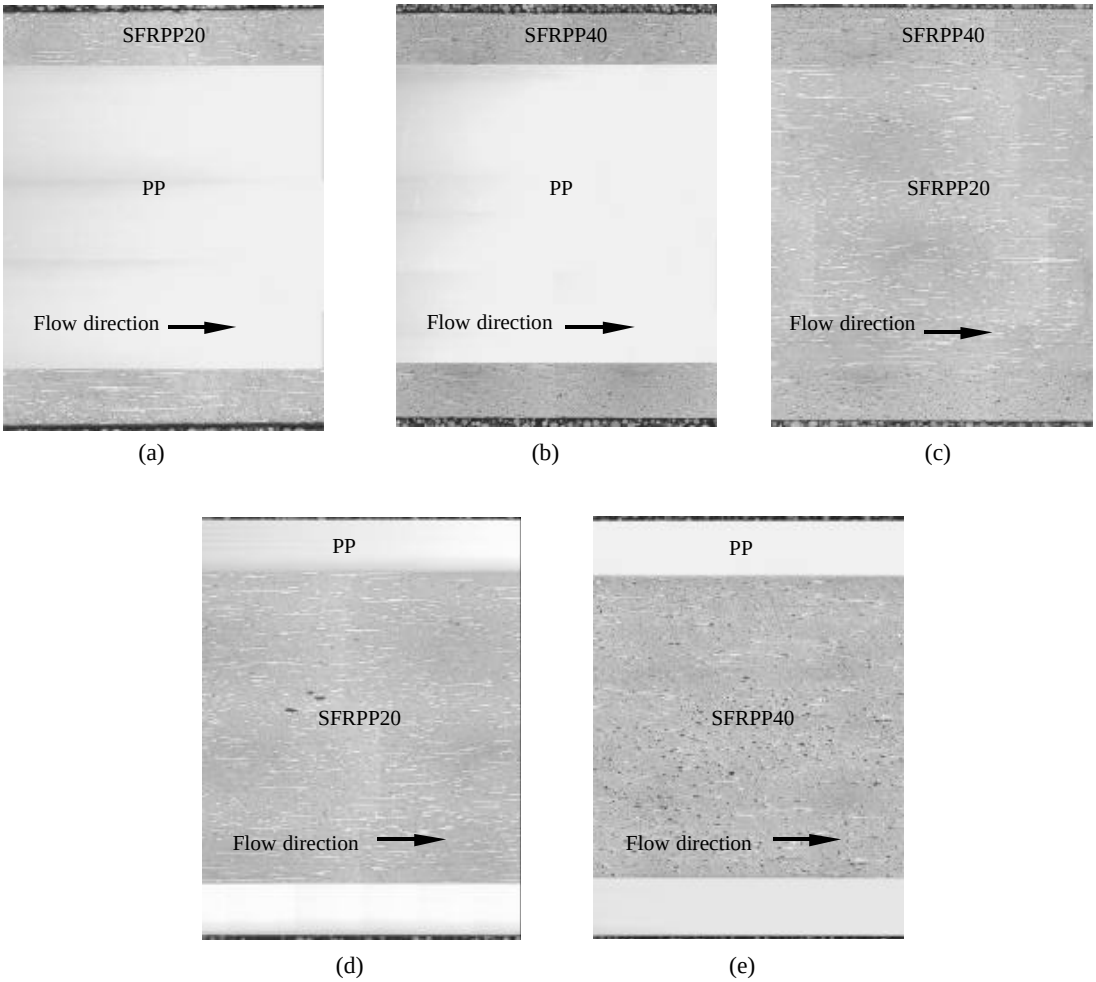

Figure 9 Optical micrographs of longitudinal area (z-y plane) of sandwich specimens: (a) SFRPP20/PP, (b) SFRPP40/PP, (c) SFRPP400/SFRPP20, (d) PP/SFRPP20, and (e) PP/SFRPP40.

The photomicrographs of longitudinal surface of sandwich specimens are illustrated in Figure 9 (a) through 9 (e). These pictures clearly indicate that the fibers are highly oriented parallel to the local flow direction within the skin region, as presented in Figures 9 (a) to 9 (c). It is interesting to note that, in the core region, it also can be observed that the higher degree of fiber orientation and lesser voids (Figures 9c-e) were thought to be caused by the shape of the velocity profile and the thickness of the frozen layer near the wall as stated earlier.

Phase Separation Analysis

Figure 10 shows the change in the percent by weight of glass-fiber inside the granules (%W_{gf}) as a function of the granular loading. It can be seen that no variation of the W_{gf} of PP filled with 20 and 40 wt% (20G and 40G) with all case of granular loading. Hence, it is clearly observed that the granular loading did not affect the homogeneity of glass-fiber inside granules, which supplied by manufacturer (BUNA).

The effect of fiber contents and the effect of different processing types on the phase distribution

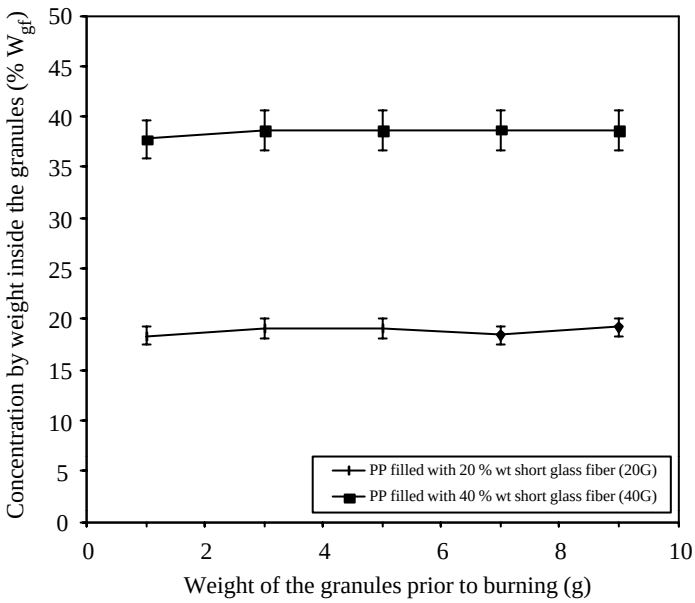

Figure 10 Weight specific analysis of granules.

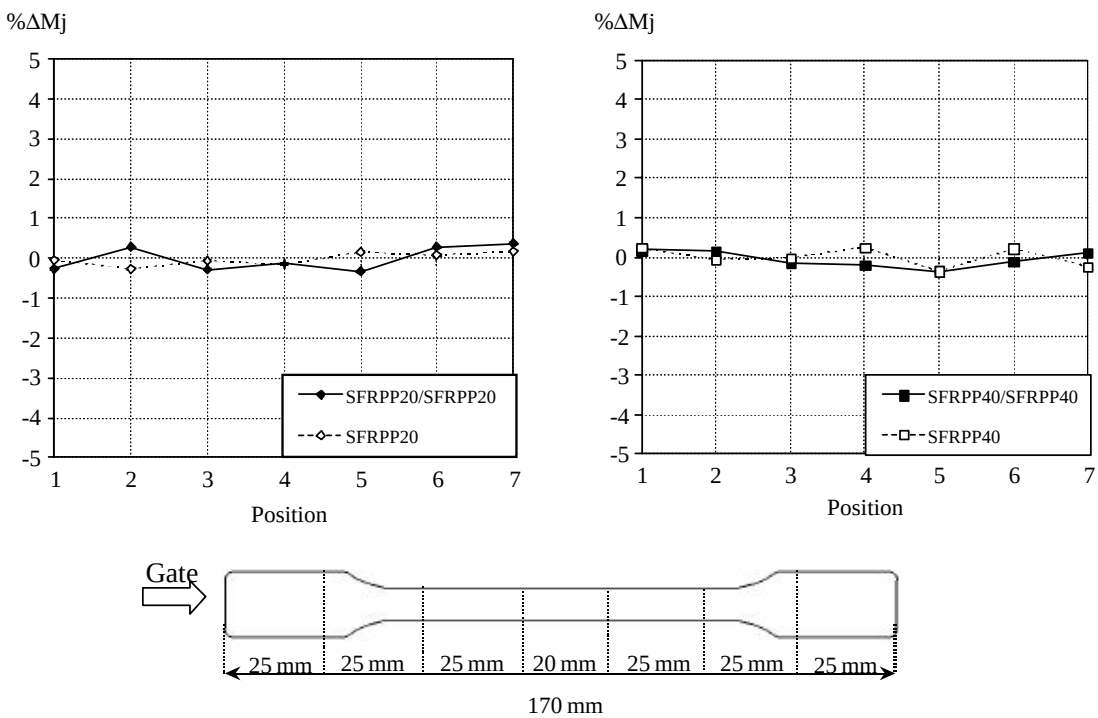

Figure 11 Comparison of phase distribution analysis of short-glass-fiber reinforced PP with sandwich and single injection molding process, at various positions of tensile specimen.

of short-glass-fiber are depicted in Figure 11. The results clearly evident that the percentage of the differences between the local filler concentration of sectioned part and the overall glass content inside the molded part (%ΔM_j) did not change with the various short-glass-fiber concentration. The results agree fairly well with the findings of Hegler *et al*. (1987) and Kubat and Szalanezi (1974). Furthermore, it was also observed that there are no significant variations of phase separation effects detectable between the both of sandwich and conventional injection molding processes. However, the inhomogeneities became considerably pronounced when using a sandwich injection process with different materials as shown in Figure 12 (different scale). For the case of SFRPP20/PP and SFRPP40/PP, it can be seen that at the region of the gate there is a shortage of glass-fibers, which finally turns into excess at the far end of the bar. In contrary to the observations made with PP/SFRPP20 and PP/SFRPP40, where the discrepancies of glass-fibers are relatively large at the far end of the bar. This could be a result of the parabolic shear flow occurring in the melt flow front of core material, as demonstrated in Figure 13. The result of changes in %ΔM_j for SFRPP40/SFRPP20 indicated that no significant difference except for the last position. It can be explained that the shortage of SFRPP20 (core material) was compensated by the skin material (SFRPP40), which have high filler contents resulting in the glass-fiber extravagance in this position.

Fiber Length Distribution

The fiber length distribution in the granules of PP filled with 20 and 40 wt % short-glass-fibers

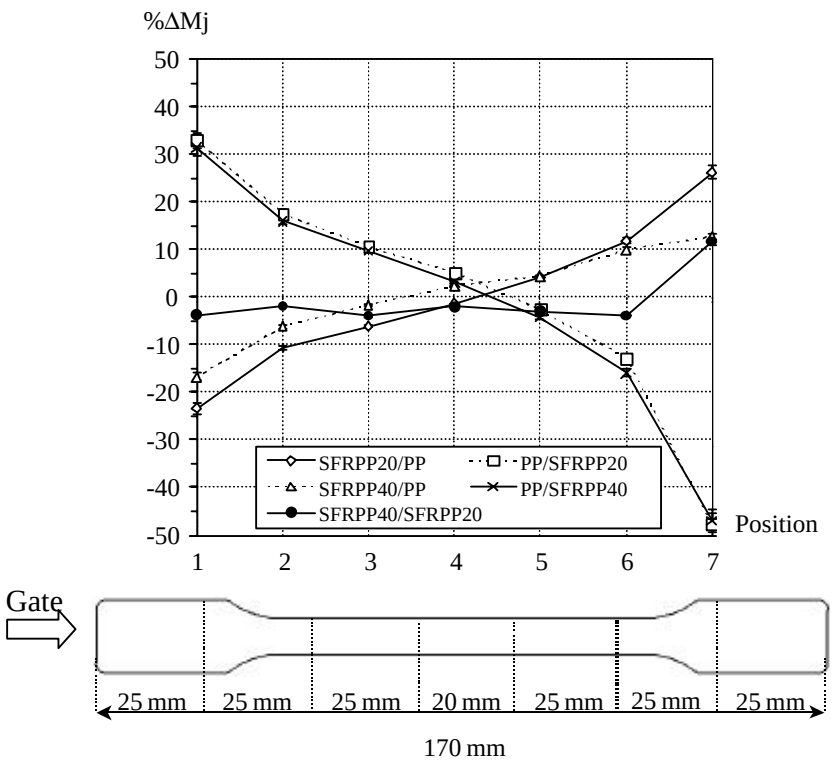

Figure 12 Comparison of phase distribution analysis of short-glass-fiber reinforced PP for sandwich injection molding process with different skin and core materials, at various positions of tensile specimens.

(20G and 40G), which supplied by manufacturer are presented in Figure 14. In general, it can be seen that the higher fiber loading, the shorter fiber length, as have been reported earlier (Fisa, 1985; Dospisil *et al*., 1994). Figure 15 (a) through 15 (c) show the percentage of the differences between a mean fiber length of pellets and the overall glass fiber length inside the molded part (%Δ*l*). In all cases, it is clear that the fiber length was much lower in the injection moldings than in the extruded compounds due to the fact that the fiber length is always reduced to a limiting value depending on melt viscosity, the intensity of the shear field and the time of treatment (Gupta *et al*., 1989). It was also clearly indicated that the mean fiber length at each subdivisions of tensile specimens decrease with the increase of glass fiber volume fraction, as observed by many authors (Singh and Kamal, 1989; Thomason, 2002) in which a higher fiber volume fraction is mainly attributed to the higher fiber-fiber interaction and higher fiber-equipment wall contact.

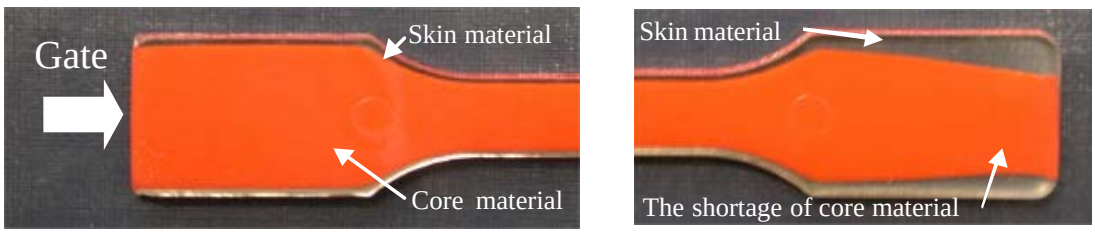

Figure 13 Flow patterns of sandwich injection molding process : (a) At the region of the gate and (b) At the far end of the bar.

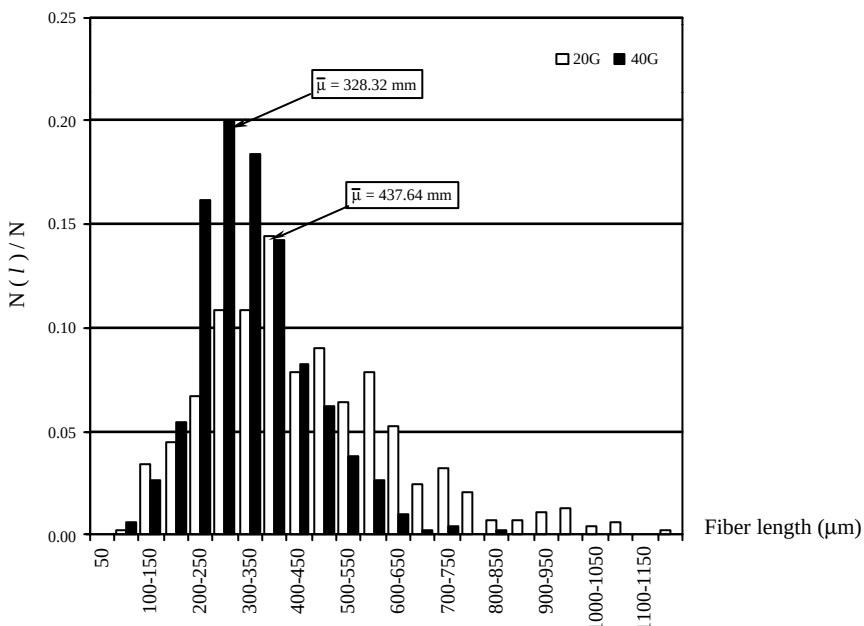

Figure 14 Histograms representing fiber length distribution of the granules PP filled with 20 and 40 wt % short-glass-fibers.

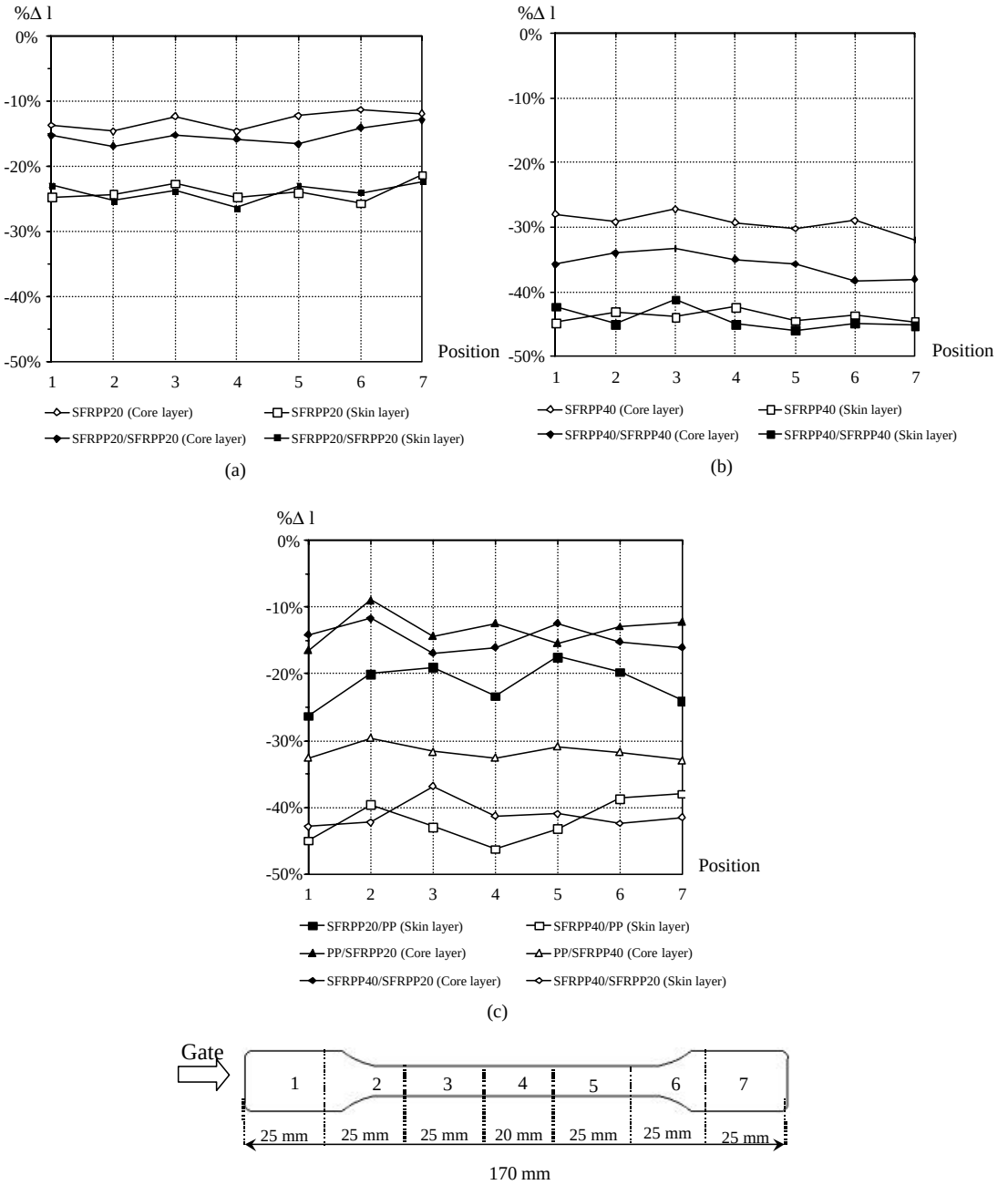

Figure 15 Fiber length distribution in the skin and the core layers at various positions of tensile specimens. (a) For single and sandwich molding processes with 20 wt % short-glass-fibers, (b) For single and sandwich injection molding processes with 40 wt % short-glass-fibers, and (c) For sandwich injection molding process with different skin and core materials.

The data in Figures 15 (a) –15 (c) also indicated that the fiber attrition inside the skin layer of injection moldings were higher than in the core layers. In our experiment, simple molded geometry, the reduction of fiber length of SFRPP20 in the core layer which was approximated to be 10-15% and in the skin layer representing about 20-25%. For the higher fiber volume fraction, the higher degrees of fiber degradation inside skin and core layers were found, approximately 30% in the core layer and 40-45% in the skin layer. However, these were not the case for this work. Karger-Kocsis and Friedrich (1987) and Baily and Kraft (1987) were also found that the skin region of the molding contained much shorter fibers than the core region due to a high shear rate near the mold surface coupled with fiber interacts with the mold geometry.

With respect to the fiber attrition in the longitude direction of the bar, it can be observed from Figures 15 (a) to 15 (c) that the effects of different processing types and glass-fiber concentration do not lead to significant changes on the fiber length reduction along the bar. In all cases, there were only insignificant differences between each subdivision. Probably cause by a simply mold gravity used for this investigation which has lesser affect on fiber length destruction along the bar, compared to a complicated geometry which has greater affect on the fiber attrition. This was due to the higher injection pressure occurred during the filling and packing processes (Hegler *et al*., 1987.

Additionally, in comparing, the effect of different processing types on the fiber length inside the skin and the core regions. From the results obtained in this work, there are only minor differences in fiber length inside skin regions observed between the both of sandwich and conventional injection molding processes. This was associated with a high shear rate near the mold surface and fiber interactions with the mold wall, as mentioned earlier. However, the effect of different processing types being more pronounced in the core region. In comparing the fiber length of SFRPP20 (Core layer) and SFRPP20/SFRPP20 (Core layer), it was interesting to observe that the fiber length distribution within the core layer of sandwich molding was slightly lower than the values obtained from single molding. For a higher fiber loading, the different values of fiber length inside the core region between SFRPP40 (Core layer) and SFRPP40/SFRPP40 (Core layer) become larger. The explanation for these would be not only related to the narrower flow channel, the higher shear rate occurred during sandwich molding process but also the higher the fiber loading, the more frequent are fiber-fiber interactions resulting in the higher fiber destruction in the core region of sandwich moldings [56].

Mechanical Properties

Figure 16 illustrates the tensile and impact properties of sandwich molding specimens containing different glass-fiber contents within skin and core materials, comparing with single molding specimens. Generally, it has been known that the addition of glass fibers resulted in a gradual increase in the tensile and impact properties (Chin *et al*., 1988, Akay and Barkley, 1991; Thomason, 2002). The mechanical properties for PP co-injected with glass-reinforced PP were generally intermediate between those of the skin and core materials alone (Messaoud *et al*., 2002). It was interesting to note that, for the sandwich molding (SFRPP20/SFRPP20 and SFRPP40/SFRPP40), the maximum tensile stress and impact strength were slightly higher than for the single moldings (SFRPP20 and SFRPP40). The increase in the mechanical properties could be due to the higher degree of fiber orientation and lesser voids within core layer, as stated earlier. However, in comparing the mechanical properties of sandwich molding and single molding, the mechanical properties of sandwich specimens are not high as one would expect. The explanation for this probably being

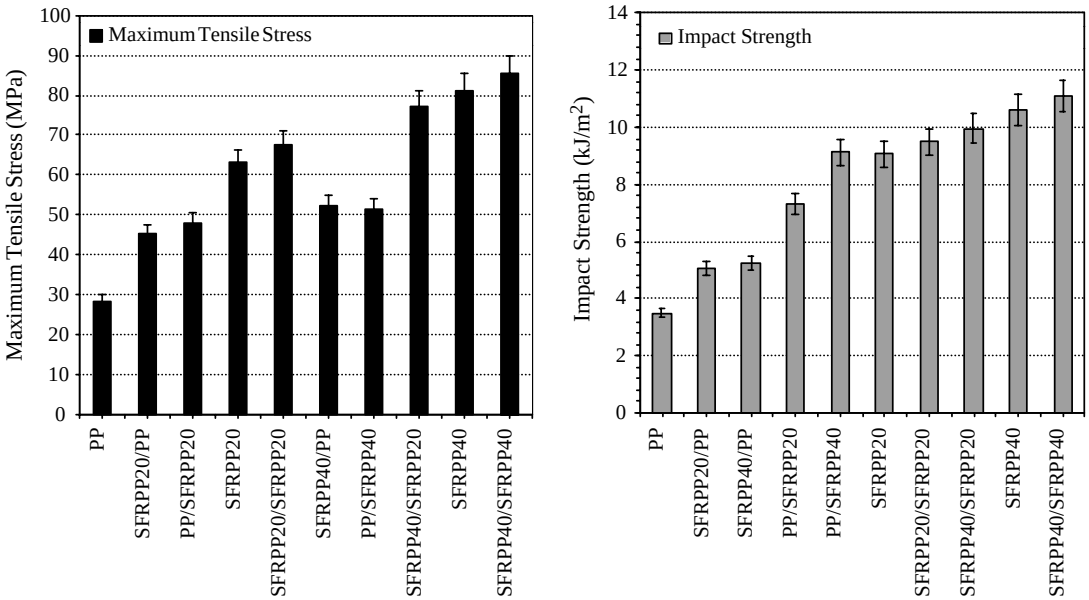

Figure 16 Effect of glass-fiber contents on maximum tensile stress and impact strength.

due to the higher fiber attrition occurred during sandwich molding process, as mention earlier and this reduction in fiber length then reduces fiber reinforcing efficiency.

Comparison of Experimental and Theoretical Results

It was essential that the experimental results of maximum tensile stress should be considered by comparing with those obtained theoretically. In this work, the theoretical prediction used was based on a rule-of–mixtures expression for the ultimate strength (UTS) of the short-fiber-reinforced composites by assuming the fiber-matrix interfacial bond is very good such that deformation of both matrix and fibers is the same (an isostrain situation). Under this condition, the total load sustained by the composite ( ) is equal to the loads carried by longitudinal fibers and transverse (or random) fibers McCrum *et al*., 1988.

$$F_C = F_L + F_T \quad (5)$$

From the definition of stress, $F = \sigma A$, and thus expressions for F_C, F_L, and F_T in terms of their respective stresses are possible. Substitution of these into Equation 3 yields

$$\sigma_{UC} A_C = \sigma_{UL} A_L + \sigma_{UT} A_T \quad (6)$$

where , , , and represent the composite, the longitudinal layer (skin material), the transverse layer (core material), and across the area, respectively. The types of molding were schematically demonstrated in Figure 17 (a). By dividing through by the total cross-sectional area of the composite, A_C and then the UTS of composite material, σ_{UC} is

$$\sigma_{UC} = \sigma_{UL} \frac{A_L}{A_C} + \sigma_{UT} \frac{A_T}{A_C} \quad (7)$$

where A_L/A_C and A_T/A_C are area fraction of skin and core regions of composite, respectively.

The ultimate tensile strength, σ_{UL} of the skin layer where fibers are parallel to the tensile axis is given by

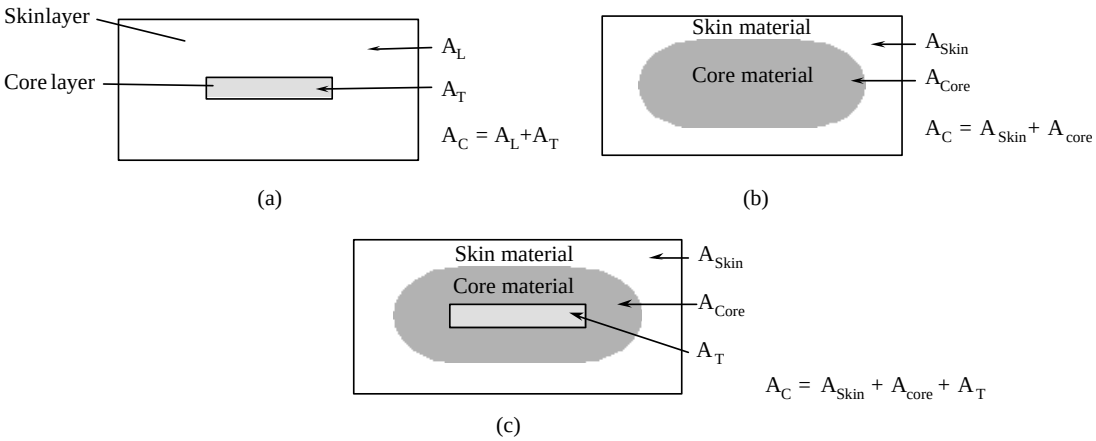

Figure 17: Schematic illustration of cross-sectional area of single and sandwich molding.

$$\sigma_{UL} = \frac{\tau l}{d} V_f + \sigma_m \left(1 - V_f\right) \qquad \text{for} < \qquad (8)$$

$$\sigma_{UL} = \sigma_f V_f \left(1 - l_c/2l\right) + \sigma_m \left(1 - V_f\right) \qquad \text{for } l \geq l_c \qquad (9)$$

where τ is interface shear strength of bondage between fiber and matrix, σ_m is the tensile strength of the matrix, V_f is the fiber volume fraction, l and d are the mean length and the diameter of the fiber, l_c is the critical fiber length $= (\sigma_f d) / 2\tau$, and σ_f is tensile strength of glass fiber (= 3.4 GPa) (Milewsky and Katz, 1987).

In the core layer, the short fibers are more likely to be randomly oriented rather than aligned. The ultimate tensile strength of the core layer, σ_{UT}, may be predicted as in [61]:

$$\sigma_{UT} = K \left(\tau l/d\right) V_f + \sigma_m V_m \qquad (10)$$

In this expression, K is a fiber efficiency parameter, which depends on V_f and σ_f/σ_m ratio. Of course, its magnitude will be less than unity, usually in the range 0.1 to 0.6. In the case of fibers randomly and uniformly distributed within three dimensions in space, the fiber efficiency parameter was taken as 0.2. Therefore, the ultimate tensile strength of the short-fiber-reinforced composites (σ_{UC}) can be evaluated with following equation:

$$\sigma_{UC} = \left\lfloor (\tau l / d) V_f + \sigma_m \left(1 - V_f\right) \right\rfloor A_T / A_C + \left(K(\tau l / d) V_f + \sigma_m V_m\right) \qquad (11)$$

The Equation 8 can also be expressed in terms of ultimate tensile strength of sandwich molding, for the SFRPP40/PP and SFRPP20/PP, as illustrated in Figure 17 (b), the σ_{UC} can be calculated from following equation:

$$\sigma_{UC} = \left\lfloor (\tau l / d) V_f + \sigma_m \left(1 - V_f\right) \right\rfloor A_{Skin} / A_C + \left(\sigma_m V_m\right) A_{Core} / A_C \qquad (12)$$

where A_{Core} and A_{Skin} are the cross-sectional area of skin and core materials, respectively. Furthermore, in the case of SFRPP40/SFRPP20, Figure 17(c), this equation can be employed as given below

$$\sigma_{UC} = \left\lfloor (\tau l / d) V_{f40} + \sigma_m \left(1 - V_{f40}\right) \right\rfloor A_{Skin} / A_C + \left\lfloor (\tau l / d) V_{f20} + \sigma_m \left(1 - V_{f20}\right) \right\rfloor A_{Core} / A_C + \left(K(\tau l / d) V_{f20} + \sigma_m V_m\right) A_T / A_C \qquad (13)$$

By substituting the parameter data (Table 4) in Equation 11, 12 and 13 the theoretically calculated results of UTS for single and sandwich

Table 4 Values for the calculations of theoretical ultimate tensile stress of short-glass-fiber-reinforced PP.

Parameter	Value									Source
	SFRPP20/PP	PP/SFRPP20	SFRPP20	SFRPP20/SFRPP20	SFRPP40/PP	PP/SFRPP40	SFRPP40/SFRPP20	SFRPP40/SFRPP40	SFRPP40	
σ_f(GPa)	3.4	3.4	3.4	3.4	3.4	3.4	3.4	3.4	3.4	[60]
τ(MPa)	14.25	14.25	14.25	14.25	14.25	14.25	14.25	14.25	14.25	[62]
σ_m(MPa)	28.5	28.5	28.5	28.5	28.5	28.5	28.5	28.5	28.5	Measured
l (μm)	500	500	500	500	500	500	500	500	500	Manufacturer
d (μm)	12	12	12	12	12	12	12	12	12	Manufacturer
V_f	0.2	0.2	0.2	0.2	0.4	0.4	0.4/0.2	0.4	0.4	Manufacturer
V_m	0.8	0.8	0.8	0.8	0.6	0.6	0.6/0.8	0.6	0.6	Manufacturer
A_L/A_C	-	-	0.92	0.96	-	-	-	0.96	0.83	Measured
A_T/A_C	-	0.04	0.08	0.04	-	0.04	0.04	0.04	0.17	Measured
A_{Skin}/A_C	0.42	0.42	-	-	0.42	0.42	0.42	-	-	Measured
A_{Core}/A_C	0.58	0.54	-	-	0.58	0.54	0.54	-	-	Measured
K	-	0.2	0.2	0.2	-	0.2	0.2	0.2	0.2	[61]

molding (σ_{UC}) are produced, these values are also compared with the results obtained from experiments shown in Figure 18. It can be seen that the values of UTS in both cases were substantially different, the predicted tensile strengths are around 1-2.5 times the measured values. The differences in the UTS values may result from the theory did not consider the effect of fiber breakage, which appears to get worse with increasing the fiber loading. A more realistic estimation of UTS may be achieved by using measured values for fiber length within skin and core layers as presented in Table 5. The mean fiber length of each layer for the complete length (seven subdivisions) of the composite part has been characterized statistically. That is,

$$\bar{\mu} = \frac{1}{j}\sum_{j=1}^{j=7}\left(\frac{1}{n}\sum_{n_f=1}^{n_f \geq 500} l_n\right), \quad j = 1,\ldots\ldots,7 \quad (14)$$

where l_n is the fiber length in each layers of sectioned parts, j the number of subdivision, and n_f is a population of the fiber length ($n_f \geq 500$).

Further substitution of the fiber length into Equation 11, 12 and 13 produced the corrected theoretical data as illustrated in Table 5, these are much closer to the experimental values. However, the corrected theoretical data are on the whole higher than the measured ones. The overestimation of UTS values may result from some parameters used in the calculation (τ and K) were given by various independent methods from literature (Vishu Shah, 1998). The conditions of the tests may be different, which would lead to an error in the calculation. Furthermore, the assumptions made in the derivation of the above equations such as the uniform fiber alignment, flaw-free molding and the assumption that the longitudinal and the transverse layers both experience the same strain, whereas these were unlikely to obtain in short-fiber-reinforced thermoplastics.

Table 5 Mean glass fiber lengths for short-glass-fiber-reinforced polypropylene.

Sample	Mean glass fiber length (μm)
SFRPP20 (Core layer)	327.65
SFRPP20 (Skin layer)	333.04
SFRPP40 (Core layer)	232.22
SFRPP40 (Skin layer)	184.38
SFRPP20/SFRPP20 (Core layer)	370.93
SFRPP20/SFRPP20 (Skin layer)	332.73
SFRPP40/SFRPP40 (Core layer)	210.95
SFRPP40/SFRPP40 (Skin layer)	183.15
SFRPP20/PP (Skin layer)	344.05
SFRPP40/PP (Skin layer)	190.68
PP/SFRPP20 (Core layer)	379.81
PP/SFRPP40 (Core layer)	224.24
SFRPP40/SFRPP20 (Core layer)	373.68
SFRPP40/SFRPP20 (Skin layer)	193.19

Table 6 Comparison of experimental, theoretical and corrected theoretical UTS for short-glass-fiber-reinforced PP made by single and sandwich injection molding processes.

Specimens	Maximum tensile stress (MPa)		
	Experimental data	Theoretical data	Corrected theorectical data
SFRPP20/PP	45.38	72.68	57.11
SFRPP40/PP	52.16	116.85	55.14
PP/SFRPP20	48.19	87.88	72.23
PP/SFRPP40	51.33	157.59	81.61
SFRPP20	63.20	133.95	96.82
SFRPP20/SFRPP20	67.58	137.75	99.37
SFRPP40/SFRPP20	77.17	185.23	107.58
SFRPP40	81.29	222.30	93.54
SFRPP40/SFRPP40	85.49	247.00	101.42

CONCLUSIONS

A sandwich injection molding technique was employed to enhance the mechanical properties of thermoplastic composites with respect to the fiber orientation and the orientation of short-glass-fibers within skin and core region. The results show that the mechanical properties are strongly dependent not only on the fiber concentration, but also on the fiber orientation, the fiber length distribution, and the voids inside the part. It is thought that the slight discrepancies in the results

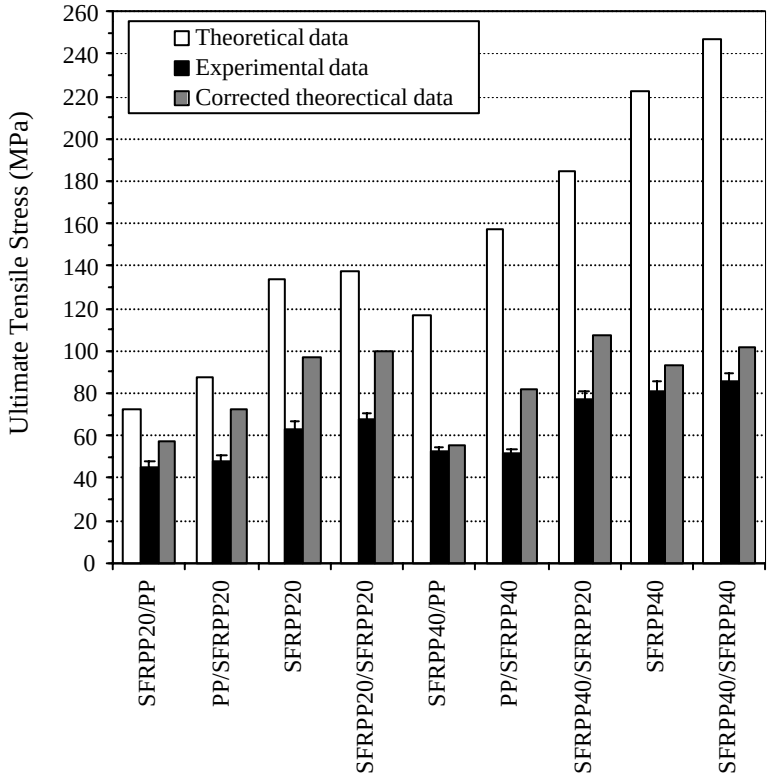

Figure 18 Comparison of experimental, theoretical, and corrected theoretical UTS of short-glass-fiber-reinforced PP.

were due to the fiber breakage occurring which depends on the mode of processing. The theoretically calculated values of UTS were found to be considerably higher than the experimental results. However, a more realistic estimation of UTS can be achieved by using measured values for fiber length within skin and core layers.

ACKNOWLEDGEMENTS

The authors are grateful to the following institutes for their kind of help: BUNA Ltd., and TARGOR Ltd. for the materials, Fakultät für Wirtschaftswissenschaften for optical microscope, Technical staff of Kunststofftechnik especially Dr.-Ing Tham Nguyen-Chung, Dipl.-Ing. Helmut Püschner and Mr. Sven Mauersberger for their technical advise.

NOMENCLATURE

Symbol	Meaning
f_p	average fiber orientation factor
f_{ps}	average fiber orientation factor in the skin region
f_{pc}	average fiber orientation factor the core region
φ_i	angle between the individual fibers and local flow direction
$N(\varphi_i)$	number of fibers with a certain angle to the local flow direction
$\%\Delta l$	percentage of the differences between a number-average fiber length of pellets and the overall glass fiber length inside the molded part
l_G	number-average fiber length inside the granule
l_j	local fiber length inside the individual layers of sectioned part
$\%\Delta M_j$	percentage of the differences between the local filler concentration of sectioned part and the overall glass content inside the molded part
M_j	local filler content
M_{tot}	average total mass of specimen
m_P	weight of specimen prior to burning off
m_G	weight of the remaining glass
n	number of sample
F_C	total load sustained by the composite
F_L	load carried by longitudinal fibers
F_T	load carried by transverse (or random) fibers
σ_{UC}	ultimate tensile stress of composite material
σ_{UL}	ultimate tensile strength of the skin layer
σ_{UT}	ultimate tensile strength of the core layer
A_C	total cross-sectional area of the composite
A_L/A_C	area fraction of skin region of the composite
A_T/A_C	area fraction of core region of the composite
τ	interface shear strength of bondage between fiber and matrix
σ_m	tensile strength of the matrix
V_f	fiber volume fraction
l	mean length of the fiber
d	diameter of the fiber
l_c	critical fiber length
s_f	tensile strength of glass fiber
K	fiber efficiency parameter
A_{Core}	cross-sectional area of core material
A_{Skin}	cross-sectional area of skin material
l_n	fiber length in each layers of sectioned part
j	number of subdivision
n_f	population of the fiber length

LITERATURE CITED

Akay M. and D. Barkley. 1991. **Journal of Materials Science** 26: 2731-2742.

Allan P.S. and M.J. Bevis 1994. **Handbook of Polymer-Fiber Composites, Polymer Science and Technology Series**. Longman Scientific & Technical: New York.

Bailey R.S. 1994. **Handbook of Polymer-Fiber Composites, Polymer Science and Technology Series**. Longman Scientific & Technical: New York.

Bailey R.S. and H. Kraft. 1987. **International Polymer Processing** 2: 94-101.

Chen S.C., K.F. Hsu and J.S. Huang. 1994. **International Communications in Heat and Mass Transfer** 21(4): 499-508.

Chin W.K., H.T. Liu and Y.D. Lee. 1988. **Polymer Composites** 5: 74-83.

Clegg D.W. 1994. **Handbook of Polymer-Fiber Composites, Polymer Science and Technology Series**. Longman Scientific & Technical. New York.

Dospisil D., J., Kubat M. Plesek and P. Saha. 1994. **International Polymer Processing** 4: 303-309.

Fisa B. 1985. **Polymer Composites** 6: 232-239.

Franzen B., C. Klason, J. Kubat and T. Kitano 1989. **Composites** 200: 65-76.

Gerard P., J. Raine and J. Pabiot 1998 **Journal of Reinforced Plastics and Composites** 17(10): 922-934.

Gogos C.G., C-F. Huang and L.R. Schmidt. 1986. **Polymer Engineering and Science** 26: 1457.

Gupta M. and K.K. Wang. 1993; **Polymer Composite** 14(5): 367-382.

Hegler, R.P., G. Mennig and C. Schmauch. 1987. **Advances in Polymer Technology** 7(1): 3-20.

Karger-Koscis, J. 1989. **Composite Materials Series: Application of Fracture Mechanics to Composite Materials**. Elsevier Science Publishers B.V.

Karger-Kocsis J. and K. Friedrich 1987. **Journal of Materials Science** 22: 947-961.

Kubat J. and A. Szalanczi. 1974. **Polymer Engineering and Science** 14: 873.

McCrum N.G., C.P. Buckley and C.B. Bucknall. 1988. **Principles of Polymer Engineering**, Oxford University Press, New York.

Meddad A. and B. Fisa. 1995. **Polymer Engineering and Science** 35(11): 893-901.

Messaoud D.A., B. Sanschagrin and A. Derdouri, 2002. ***SPE ANTEC* Technical Papers** 645-648.

Milewsky J.V. and H.S. Katz, 1987. **Handbook of Reinforcements for Plastics**. Van Nostrand Company Limited, New York.

O′ Regan D.F., R.S. Bailey and M. Akay. 1995. **Composite Science and Technology** 55: 109-118.

Pechulis, M. and Vautour, D. 1997. **SPE ANTEC Technical Paper** : 1860-1864.

Schlatter G., J.F. Agassant, A. Davidoff and M. Vincent. 1999. **Polymer Engineering and Science** 39(1): 78-88.

Seldezn, R. 2000. **Polymer Engineering and Science** 40(5): 1165-1176.

Tadmor Z. 1974. **Journal of Applied Polymer Science** 18(6): 1753-1772.

Thomason J.L. 2002. **Composites: Part A** 33: 1641-1652.

Vishu Shah. 1998. **Handbook of Plastics Test Technology**, 2nd ed. John Wiley & Sons, Inc.,

ZOLTEX Companies, INC., 2000. ST.Louis, MO 63044, **User ‘s guide for short carbon fiber composites**, June.